Quantitative Analyses of Small-Angle X-ray Scattering Profiles with a Linear Position Sensitive Detector

By

Mineo FUJIMURA, Takeji HASHIMOTO and Hiromichi KAWAI

(Received December 27, 1980)

Abstract

Quantitative data analyses of small-angle scattering (SAXS) profiles measured with a linear position sensitive detector (PSD) are discussed. We shall describe corrections of the measured SAXS profiles for (i) non-uniformity of the detector sensitivity along its length, (ii) collimation errors, and (iii) reduction of the position resolution due to the oblique incidence of photons to the detector. The correction of the profile for the collimation errors (i.e., desmearing) involves measurement of the slit weighting functions which depend on properties related to the PSD and its electronics (e.g., channel number or conversion gains of ADC and TAC, position resolution, and the uniformity of detector sensitivity) as well as the optical set-up of the SAXS apparatus. It is shown that properly corrected SAXS profiles obtained with the PSD quantitatively agree with those obtained with a conventional step-scan SAXS apparatus such as the Kratky U-slit system and the Beeman four slit system.

I. Introduction

The small-angle X-ray scattering (SAXS) technique has greatly advanced with the developments of the position sensitive detectors (PSD) and related electronics. The measuring time for the SAXS profiles has been greatly reduced, roughly two orders of magnitude, by the use of the PSD, thus permitting dynamic studies of structure formation during crystallization[1] or phase-separation in multi-component systems[2]. The SAXS apparatus with the PSD is superior to those with conventional step scan devices as regards the following aspects: (i) scattered intensity is simultaneously detected over many scattering angles so that the relative scattered intensity profile is not distorted by fluctuations of the incident beam intensity, and (ii) errors in photon-counting due to the finite dead time of the electronics and counters (order of 10 μ sec. in our case) are equivalent for all channels (i.e. the scattering angles) so that they do not also disturb the relative intensity distribution.

Department of Polymer Chemistry

Although the PSD is an efficient and powerful detector for the SAXS measurements, one has to correct the scattering profiles measured with the PSD for the various factors which we shall discuss below in order to obtain the "desmeared" profiles or true scattering profiles. In this paper we shall discuss the corrections of the measured profiles for the non-uniformity of the detector sensitivity along its length, collimation errors, and the reduction of the position resolution due to the oblique incidence of the scattered photons to the detector.

The correction of the profile for the collimation errors[3,4] involves measurement of the slit weighting functions which depend on the factors related to the properties of the PSD and its electronics (e.g. channel numbers used for a particular experiment, position resolution and the sensitivity of the detector) as well as the optical set-up common to all the apparatuses. In this paper we shall quantitatively compare the desmeared scattering profile obtained with the PSD with those obtained with conventional step-scan apparatuses, such as the Kratky *U*-slit system[5] and the Beeman four-slit system[6], in order to investigate feasibility of obtaining quantitative data with the PSD.

II. Apparatus

Complete details of the apparatus will be described elsewhere.[7] We just briefly describe its outline below. We use a 12 kW rotating anode X-ray generator as a source of the incident X-ray beam. The beam is monochromatized with a graphite crystal and a pulse-height analyzer to CuKα radiation. The scattered X-ray beam was detected by a linear position sensitive proportional counter (a multicathode delay line PSD, Rigaku-Denki) filled with PR gas (Argon 90 % and Methane 10 %). The PSD has an effective length of 50 mm, a depth of 11.0 mm (along the incident beam) and a window height of 10 mm, the height of the window being varied by inserting height-limiting slits. The effective length is resolved into many channels, the number of channels being determined by conversion gains of the time-to-amplitude converter (TAC) and of the analogue-to-digital converter (ADC). The maximum conversion gain of the ADC is $1024/8V$, thus the effective length is resolved into 1024 channels (chs.). For example by increasing the gain of the TAC from $8V$/50 mm to $8V$/12.5 mm one quarter of the effective length can be resolved into 1024 chs., which is equivalent to further increasing the detector-resolution by four times (4096 chs.).

III. Fundamental Data on PSD

III-1. Uniformity of the Detector Sensitive

The uniformity of the detector sensitivity along its length was measured by

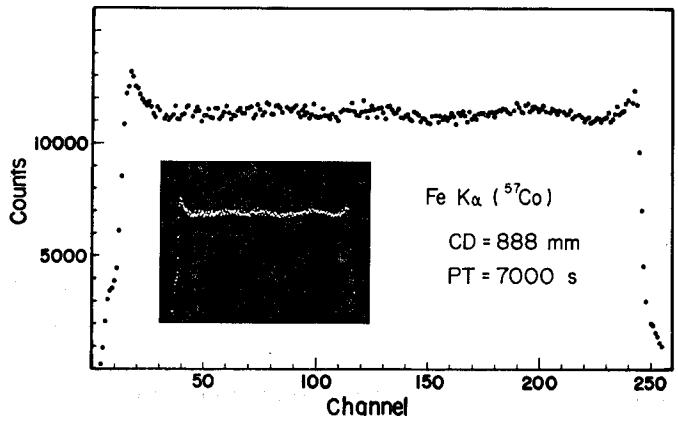

Fig. 1. Uniformity of the sensitivity of the PSD along its length as measured by FeKα radiation from 2mCi ^{57}Co. Measuring time 7000 sec., 256 chs., specimen to detector distance (CD) 888 mm.

FeKα radiation (6.4 keV) from 2mCi ^{57}Co. Figure 1 shows an oscilloscope display of photon counts along the detector length measured with 256 channels (chs), the sample-to-detector distance 888 mm, and measuring time 7000 sec. It is shown that the sensitivity is uniform within $\pm$3.5 % over 224 chs., except for the two edges of 18 chs. The non-uniformity is very reproducible, and therefore the data can be used as a calibration to correct for the non-uniformity. We construct a set of calibration curves for various channel numbers used in the experiment. We discard the data obtained at the edge regions of the detector.

III-2. Channel Number and Position of the Photons

The relationship between the channel number of the detector and position of

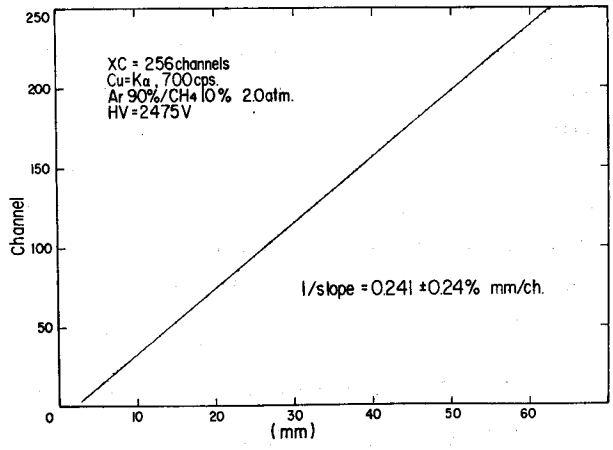

Fig. 2. The relationship between the channel number of the detector and position of incident photon.

photon was measured by shifting the PSD relative to a narrow slit placed in front of the detector, and by finding the channel number having a maximum intensity. The result is shown in Figure 2 where it is found that the relationship is linear within ± 0.24 %. This relationship was used to convert the channel number into the real position on which the photon falls. The conversion factor depends, of course, on the conversion gains of ADC and TAC.

III-3. Position Resolution of PSD

The position resolution of the detector was estimated by measuring the profiles of the scattered X-ray beam through a fine slit of 50 μm width, which is put in front of the detector. Figure 3 shows the profile of the X-ray beam through the

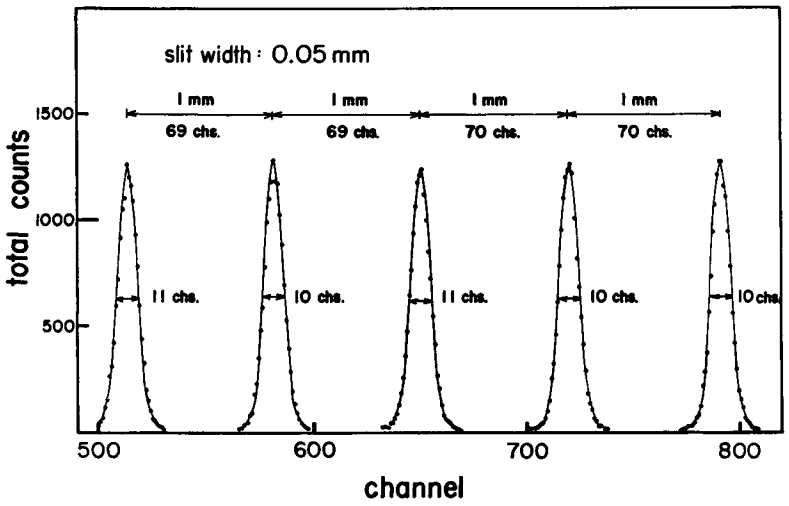

Fig. 3. Position resolution of the detector along its length, measured with 4096 chs..

slit as a function of the position of the detector, the detector being displaced relative to the slit. The scattered X-ray beam used for this purpose has a broad distribution so that the intensity essentially remains constant over a 50 μm slit width. The profiles were measured with 4096 chs. by increasing the conversion gain of TAC (from 8V/50 mm to 8V/12.5 mm). It is concluded that the position resolution of the detector is constant throughout the detector. The *FWHM* is 10~11 chs. or 0.142~0.156 mm. If the true position resolution of the detector is given by the Gaussian function, $R_D(x)$, with the standard deviation σ_D, then σ_D is estimated from the measured profile as defined by $R_{obs}(x)$:

$$R_{obs}(x) = S(x) * R_D(x) \quad (1)$$

$$R_D(x) = (2\pi\sigma_D^2)^{-1/2} \exp(-x^2/2\sigma_D^2) \quad (2)$$

where the asterisk * designates a convolution product defined as

$$S(x)*R_D(x) = \int dt\, S(t) R_D(x-t)$$

and $S(x)$ is the slit function which is approximately equal to a step function of width the 50 μm. The value of σ_D thus estimated is 59 μm. Figure 4 shows a

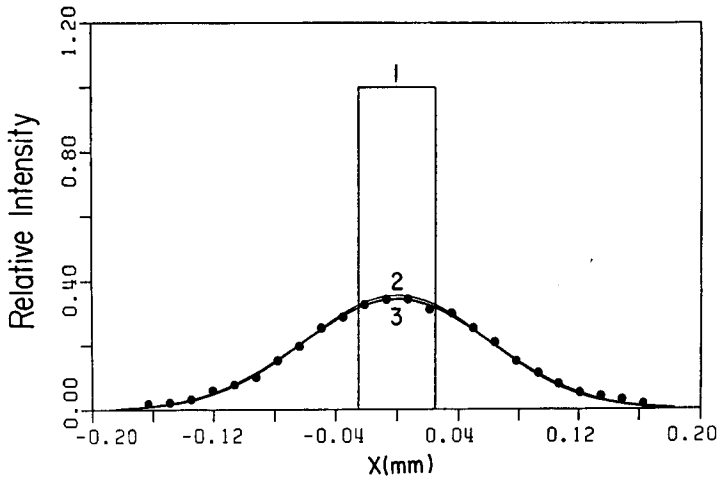

Fig. 4. Measured (solid circles) and estimated profile $R_{obs}(x)$ (solid line #3) of the X-ray beam through slit of width 50 μm. The estimated profile assumes the Gaussian resolution function of eq. (2) with σ_D=59 μm. The Gaussian resolution function $R_D(x)$ (solid line #2, σ_D=59 μm) and the slit function $S(x)$ (line #1, 50 μm width) are also included.

comparison of the measured data (solid circles) with the estimated profile $R_{obs}(x)$ (solid line #3, σ_D=59 μm), the Gaussian resolution function $R_D(x)$ (solid line #2, σ_D=59 μm) and the slit function $S(x)$ (solid line #1). The position resolution affects the slit-weighting function $W(u_1, u_2)$ of the SAXS system. A fine agreement is obtained between the measured profile and the estimated profile R_{obs}, indicating that the resolution function of the detector is given by a Gaussian function with a standard deviation σ_D=59 μm.

III-4. Resolution Reduction due to Oblique Incidence

When photons make an oblique incidence to the detector the photons may ionize the PR gas, as schematically shown in Figure 5, so that the incident photons affect not only the counting rates at channel i but also the counting rates of other channels (e.g., j-channel), resulting in the resolution reduction. The resolution reduction depends on the scattering angle 2θ and the depth of the detector d_t, and

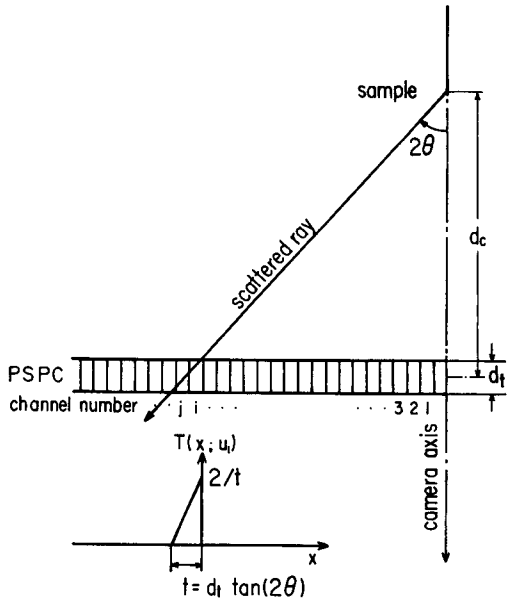

Fig. 5. Schematic diagram showing a resolution reduction of the detector due to an oblique incidence of photon. 2θ: scattering angle of incident photon, i: channel number at which photon falls, d_t: depth of the detector, $T(x; u_1)$: the smoothing function associated with the resolution reduction. $t=d_t \tan 2\theta=(d_t/d_c)u_1$.

the larger the values of 2θ and d_t, the greater is the effect.

In order to investigate the effect, we tilted the detector with respect to the incident beam and observed the profile of the incident beam through a narrow slit of 50 μm width placed in front of the detector as a function of the tilt angle. The incident beam used in this experiment has essentially a constant intensity over 50 μm slit width. Figure 6 shows the result as a function of the tilt angle 2θ. It is clearly shown that the *FWHM* increases with increasing the tilt angle due to the resolution reduction. We may approximate the observed profile $O_{obs}(x; u_1)$ at a given u_1 (the coordinate along the detector which specifies the position of the incident photon, $\tan 2\theta=u_1/d_c$) by a function $P(x; u_1)$ given by

$$\begin{aligned} P(x; u_1) &= T(x; u_1)*R_{obs}(x) \\ &= T(x; u_1)*S(x)*R_D(x) \end{aligned} \qquad (3)$$

where $T(x; u_1)$ is a normalized function as defined in Figure 5, and $R_{obs}(x)$ is the observed profile of the incident beam through the slit of 50 μm width under the normal incidence (eq. 1).

Figure 7 compares the measured profile $O_{obs}(x; u_1)$ (solid circles) with the

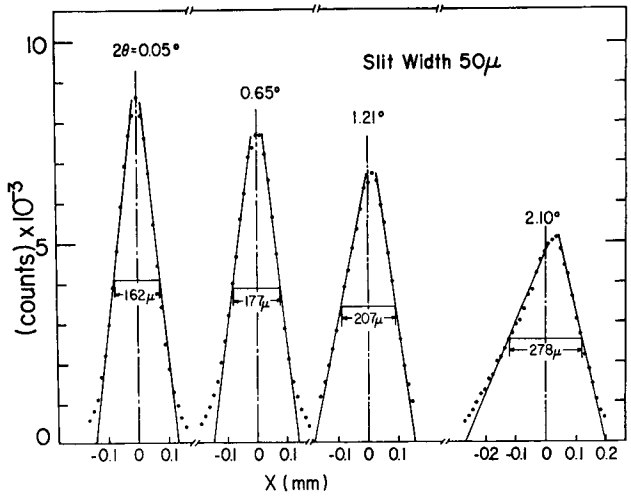

Fig. 6. Measured resolution reduction due to an oblique incidence as a function of incident angle 2θ.

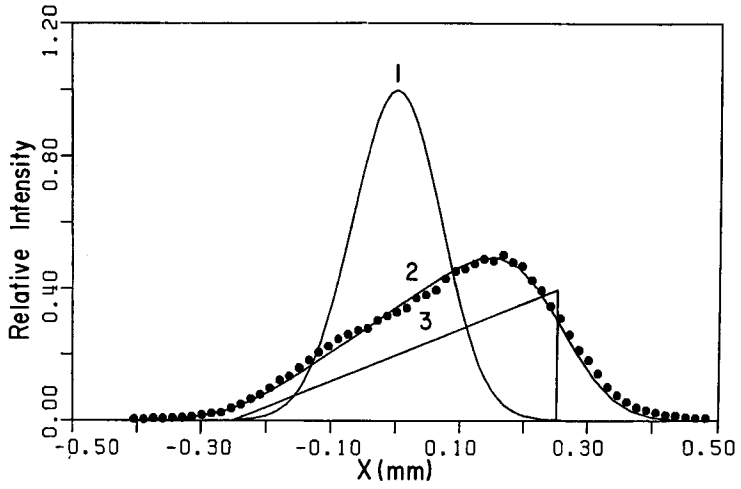

Fig. 7. A comparison between measured profile $O_{obs}(x; u_1)$ (solid circles) and estimated profiles $P(x; u_1)$ (curve #2), $T(x; u_1)$ (curve #3) and $R_{obs}(x)$ (curve #1) for a given oblique incidence of $2\theta=2.62°$, or $u_1=40.3$ mm ($d_c=880$ mm).

estimated functions $P(x; u_1)$ (solid line #2), $T(x; u_1)$ (solid line #3) and $R_{obs}(x)$ (solid line #1) for a given oblique incidence of $2\theta=2.62°$ or $u_1=d_c \tan 2\theta=40.3$ mm ($d_c=880$ mm). An extremely fine aggreement was obtained between $O_{obs}(x; u)$ and $P(x; u_1)$, indicating that the triangular function $T(x; u_1)$, determined purely from geometrical factors (as seen in Figure 5), describes the resolution reduction due to the oblique incidence of photons. Figure 8 shows a comparison between

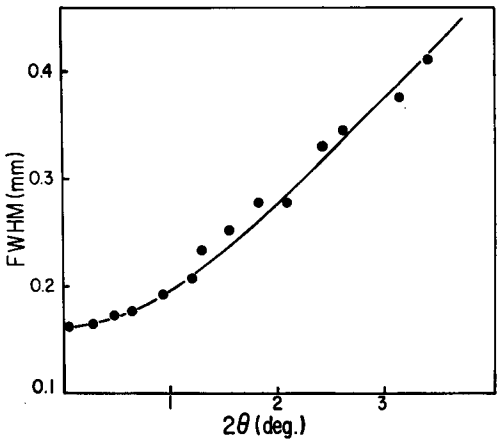

Fig. 8. A comparison between measured (solid circles) and calculated (solid line) *FWHM* of the profiles of the incident beam through a slit of 50 μm width as a function of the tilt angle 2θ.

the measured (solid circles) and calculated (solid line) *FWHM* of the profiles of the incident beam through the slit of 50 μm width as a function of the tilt angle 2θ. Again a fine agreement between them is obtained over a wide range of 2θ.

We define a general "smoothing function $O(x; u_1)$" at a given channel u_1, associated with the resolution reduction due to the oblique incidence. The function $O(x; u_1)$ which turns out to be equal to $T(x; u_1)$, with a high accuracy from the results of Figures 7 and 8, is a function obtained with a detector having an ideal position resolution, i.e., $\sigma_D=0$. We first make corrections for the finite position resolution of the detector. (This process is the so-called desmearing process as discussed in section IV). Then the *SAXS* profile smeared by the effect of oblique incidence only, $I_{obl}(s)$, may be related to the true or unsmeared intensity $I(s)$ by an integral equation (see Figur 9):

$$I_{obl}(s) = \int_{-\infty}^{\infty} du_1 I(u_1) O(s-u_1; u_1) \tag{4}$$

We should note that $O(x; u_1)$ is a function of the channel number u_1 and that

$$\int du_1 O(x; u_1) = \text{(constant)} \tag{5}$$

It is obvious that the resolution reduction due to the oblique incidence is increasingly significant with increasing the scattering angles. (See Figure 8.) The effect, however, is almost negligible at very small angles (small than 40 minutes

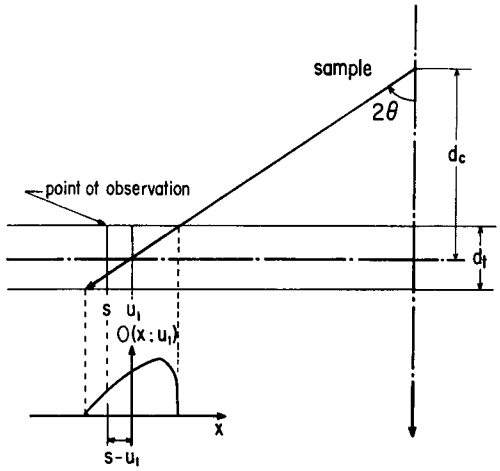

Fig. 9. A diagram showing a principle to calculate an effect of the resolution reduction on the SAXS profile. $O(x; u_1)$ is a smoothing function at a given channel u_1 associated with the resolution reduction due to the oblique incidence. u_1 is the coordinate along the detector length correspondoing to the scattering angle 2θ, i.e., $u_1=d_c \tan 2\theta$.

in the scattering angle). Consequently, in the following analyses we shall not include the correction for the resolution reduction due to the oblique incidence.

IV. Desmearing

The true intensity I_{obs} is related to the measured intensity $\tilde{I}_{obs}$, corrected already for the non-uniformity of the detector sensitivity and resolution reduction due to the oblique incidence of photons by Fredholm's integral equation of the first kind;

$$I_{obs}(s) = \int_{-\infty}^{\infty}\int_{-\infty}^{\infty} du_1 du_2 W_H(u_2) W_W(u_1) \tilde{I}_{obs}([(s-u_1)^2+u_2^2]^{1/2}) \qquad (6)$$

where W_H and W_W are the slit-length and slit-width weighting functions. The "desmearing" process to obtain I_{obs} from $\tilde{I}_{obs}$ is composed of two processes, i.e. evaluation of the weighting functions and finding the solution of the integral equation. The two processes for the conventional step-scan goniometers were fully described in our earlier paper[8]. (We measured and/or calculated the weighting functions and desmeared by using an iterative method.)

We also desmear the profiles measured with the PSD by the same iterative method. We describe below the measurements of the weighting function for the apparatus with the PSD.

Hendricks and Schmidt have shown that the weighting function $W(\boldsymbol{u})$ where $\boldsymbol{u}=(u_1, u_2)$ is given by a convolution product of intensity distribution of the incident beam at the detector plane $i_0(\boldsymbol{u})$ and spatial distribution of the detector sensitivity $e(\boldsymbol{u})$ in a case when there are no slit edges between the sample plane and the detector plane

$$W(\boldsymbol{u}) = i_0(\boldsymbol{u}) * e(\boldsymbol{u}) \tag{7}$$

The function $e(\boldsymbol{u})$ is a fixed function and independent of the scattering angles for the apparatus with a step-scanning goniometer. On the other hand, $e(\boldsymbol{u})$ for the PSD is not a fixed function but in general depends on scattering angles or channel numbers. In the case of the PSD, the function $e(\boldsymbol{u})$ is a function of the width of the channel determined by the conversion gain of ADC and TAC, and also the position resolution of the detector itself, i.e., $R_D(\boldsymbol{u})$ in eq. (2):

$$e(\boldsymbol{u}) = S_e(\boldsymbol{u}) * R_D(\boldsymbol{u}) \tag{8}$$

where $S_e(\boldsymbol{u})$ is a step function with a width determined by the conversion gains of ADC and TAC and the effective area of the detector along its length and width.

The function $S_e(\boldsymbol{u})$ is obviously independent of the channel number, i.e. the scattering angle, and so is the function $R_D(\boldsymbol{u})$ from the experimental result as shown in Figure 3. Therefore, the function $e(\boldsymbol{u})$ is essentially independent of the scattering angle for our detector, just as in the case of the conventional step-scanning apparatus. Consequently, the weighting function $W(\boldsymbol{u})=W(u_1, u_2)$ is identical to the profile of the center beam measured with the PSD under given conditions, i.e. under the given conversion gains of ADC and TAC, the window height of the PSD, and the optical set-up.

Figure 10 shows 1/4 of the weighting function measured with the PSD. The effective length is resolved with 256 chs. and the window height of the detector is 10 mm. The corresponding optical set-up is shown in Figure 11 (a). The coordinates u_1 and u_2 are those along the slit-width and the slit-length. The function is measured as follows: the intensity profile of the center beam was measured with 256 chs. at a given u_2, the measured profile of which is nothing other than the weighting function at that u_2. We then shift the detector along the slit length direction to another u_2, the profile of which is equal to the weighting function at that u_2. The weighting function obviously depends on the PSD and its related electronics such as (i) number of channels, position resolution, uniformity of the detector sensitivity, height of the window, and energy resolution of the detector as well as the optical set-up of the SAXS apparatus. If one of these variables is

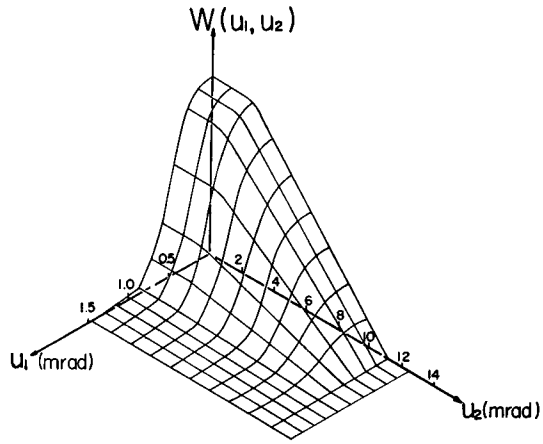

Fig. 10. Measured slit weighting function $W(u_1, u_2)$ of the SAXS apparatus with the PSD, where u_1 and u_2 are the coordinates along slit-width and slit-length directions, respectively. 256 chs.

changed, the weighting function obviously changes and should be measured again. We can easily show from Figure 10 that

$$W(u_1, u_2) = W_W(u_1) W_H(u_2) \tag{9}$$

V. Comparison of Desmeared Curves

V-I. Optical Set-Up

Figure 11 shows a comparison of the optic systems of three SAXS apparatuses where (a) is the system with PSPC, (b) is the four-slit system with Soller slits between the third and fourth slits, and (c) is the Kratky U-slit system. CuKα radiation was used for all the systems. The systems (a) and (b) use the rotating anode X-ray generator (RU-z and —a, Rigaku Denki operated at 200 mA and 40 kV). System (a) uses a point-focussing with an effective focal-sopot size 1.0×0.5 mm^2 at a take-off angle of 6°, and the source was monochromatized by a graphite monochromator. The higher-order harmonics of Bremstrahlung is cut-off by the pulse-height analyzer in the PSD electronics.

System (b) utilizes the line-focussing with an effective focal spot size of $0.05 \sim 10$ mm^2 at 6° take-off. The incident beams were monochromatized by a N_i-filter and a pulse-height analyzer. System (c) utilizes the Phillips broad-focus X-ray tube with the focal spot of 12 mm in length. The incident beam was monochromatized as in system (b).

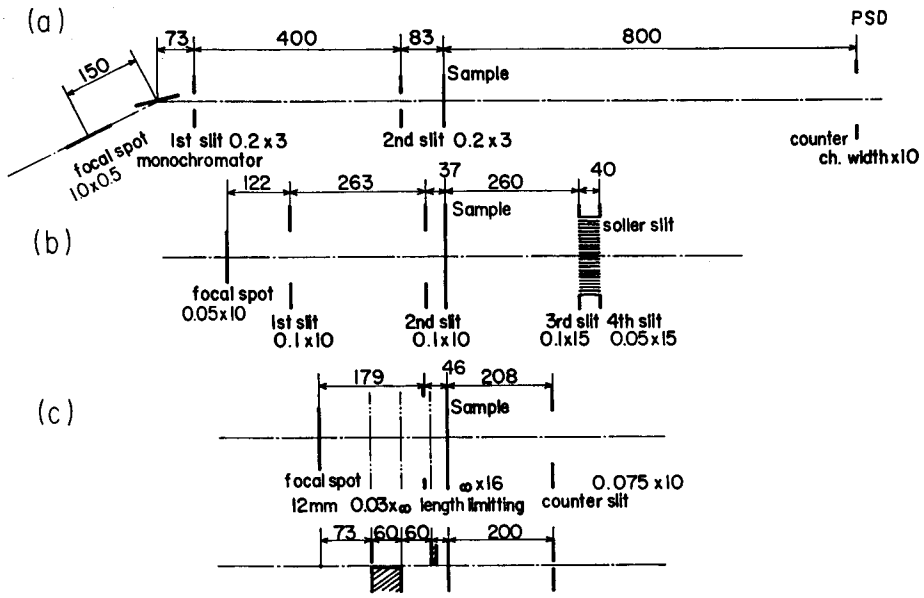

Fig. 11. Optical systems of the three SAXS apparatuses: (a) a system with the PSD, (b) four-slit system with Soller slits between the third and fourth slits, and (c) Kratky U-slit systems.

V-2. Weighting Functions

The weighting functions for the step-scanning systems of Figures 11(b) and 11(c) are estimated (calculated and/or measured) as described in detail by Todo, Hashimoto, and Kawai[8]. The function for the PSD system has already been discussed in the preceeding section.

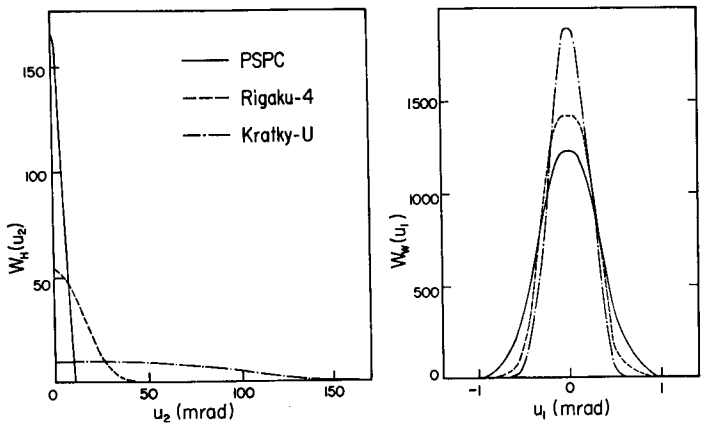

Fig. 12. Comparisons of the slit-height $W_H(u_2)$ and slit-width $W_W(u_1)$ weighting functions for the three SAXS systems.

Figure 12 shows comparisons of the weighting functions of the three optical systems along the slit-height, $W_H(u_2)$, and along the slit-width $W_W(u_1)$. The slit-width weighting functions are not very different, but the slit-length weighting functions are very different.

V-3. Comparisons of Some Scattering Profiles

Figure 13 shows a comparison of measured scattering curves ($\tilde{I}_{obs}$) and desmeared scattering curves (I_{obs}) in arbitrary intensity units for the standard Lupolen

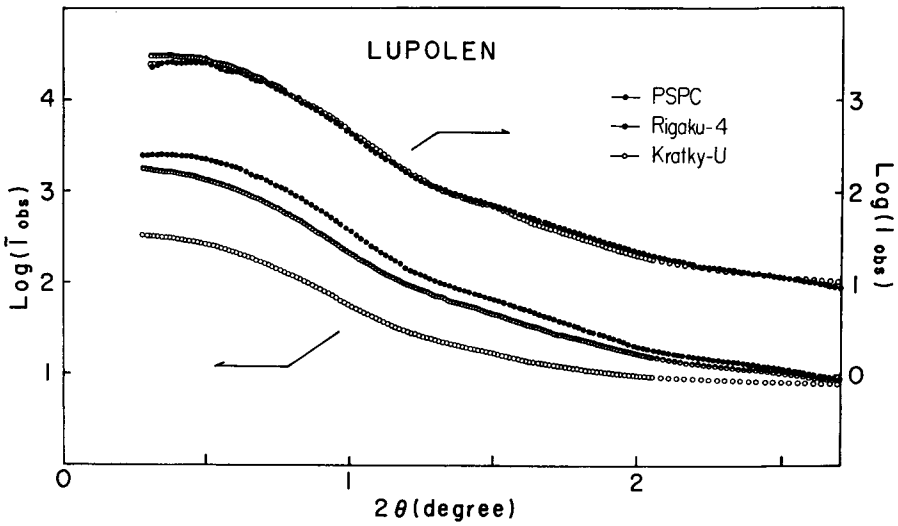

Fig. 13. A comparison of measured scattering curves $\tilde{I}_{obs}$ and desmeared scattering curves I_{obs} (both in arbitrary intensity units) for the standard Lupolen sample, 256 chs., 300 sec. measuring time.

sample, a polyethylene film used for calibration of the absolute intensity. The measuring time was 300 sec., and the full length of the detector was resolved into 256 chs. in the PSD system. The measured curves of the three systems are very different due to the differences in the weighting functions. However, the desmeared curves are quantitatively identical as shown in the figure. The data are corrected for sample absorption and background scattering (i.e., air and/or parasitic scattering).

Figure 14 shows a comparison of measured and desmeared scattering curves for a particular diblock polymer of styrene and isoprene having spherical microdomains (total molecular weight 2.0×10^5, weight faction of styrene in the polymer 0.87, heterogeneity index $\bar{M}_w/\bar{M}_n=1.18$). The profile with the PSD system was obtained with 256 chs. and with a measuring time of 4000 sec. The morphology

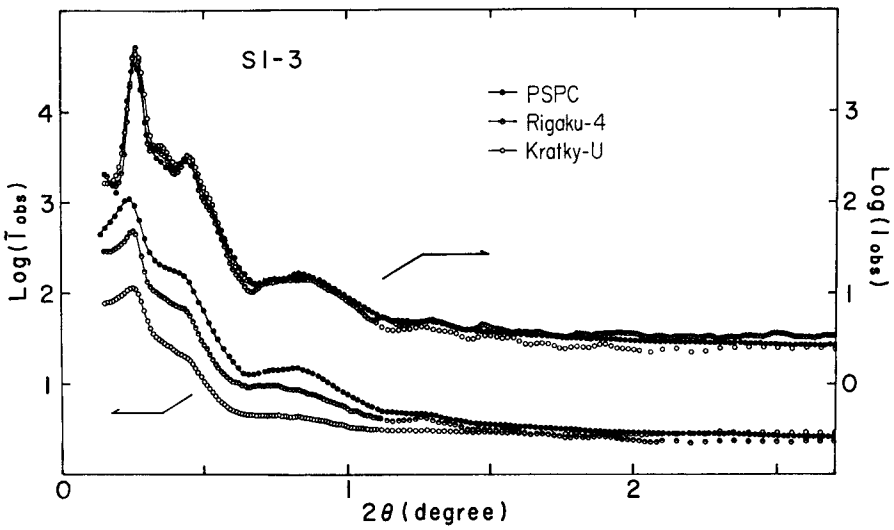

Fig. 14. A comparison of measured and desmeared scattering curves for a particular diblock polymer of polystyrene and polyisoprene (SI-3) having spherical microdomains. 256 chs., 4000 sec. measuring time.

of the block polymer and nature of the microdomains are fully described elsesewhere[9-12]. The spatial arrangement of the spherical microdomains is quite regular, forming, more or less, simple-cubic-like macrolattice. Consequently, it gives a number of scattering maxima arising from interparticle interference.

The first-order peak which appears at the scattering angle $2\theta=15.6$ min. is associated with the nearest-neighbour distance D between the sphers. The peaks appear at the scattering angles 21.0, 26.4, and 33 min., each of which corresponds, respectively, to that at $\sqrt{2}$, $\sqrt{3}$ and $\sqrt{4}$ of the scattering angle of the first order peak. The broad peaks at $2\theta=51$ and 78 min. are the first-order and the second-order scattering maxima arising from an isolated sphere. (The quantitative analyses of the scattering profile indicates that the size distribution may be described by a Gaussian function with a standard deviation of 11 % of its average radius[12]). It is shown that the desmeared curves are nearly identical to one another, but that the second peak at the scattering angle of $\sqrt{2}$ of the first peak is unresolved in the curve measured with the PSD system. This may be due to the fact that the channel number 256 is not sufficient for this intensity profile. In order to confirm this point we measured the scattering profile with 512 channels, the result of which is shown in Figure 15.

Figure 15 shows a comparison of the desmeared scattering profile obtained from the PSD system with those obtained from the two conventional step-scanning apparatuses, for the same film specimens as in Figure 14. (The measuring time

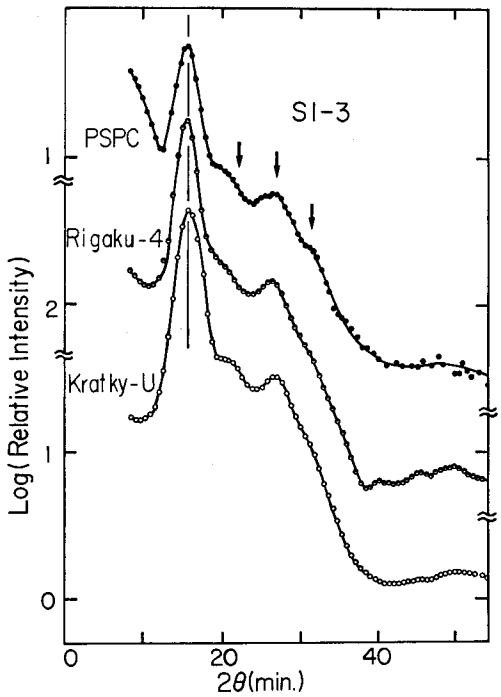

Fig. 15. A comparison of desmeared scattering curves for the polystyrene-polyisoprene diblock polymer SI-3, the same specimen as in Figure 14. The SAXS profile from the PSD system was obtained with 512 chs.

was 800 sec., and the number of chs. for the PSD system was 512 chs.). It is clearly indicated that all the scattering maxima are clearly resolved with the PSD system. The first-order peak and the peaks at $\sqrt{2}$, $\sqrt{3}$, and $\sqrt{4}$ of the first peak quantitatively agree with those obtained by the step-scanning goniometers. The excess scattering which appears in the profile obtained from the PSD system at very small angles is due to a parasitic scattering which can be easily eliminated.

Therefore, from this study, we can conclude that the PSD is very useful and efficient for obtaining very quantitative SAXS profiles, as well as for application to high-speed dynamic measurements[1,2,7]. One can reduce the measuring time approximately by two orders of magnitude by using the PSD.

Acknowledgement

This work was supported by a Grant-in-Aid for Scientific Research (243021 and 449012) from the Ministry of Education, Japan. The authors thank Dr. F. Hamada and Dr. H. Hayashi, Department of Polymer Chemistry, Kyoto Univer-

sity, Kyoto, Japan for kindly arranging the SAXS measurement with the Katky Camera.

References

1) J.H. Schultz, J.S. Lin, and R.W. Hendricks, J. Appl. Cryst., **11**, 551 (1978).
2) T. Hashimoto, Y. Tsukahara, and H. Kawai, J. Polym. Sci., Polym. Lett. Ed., **18**, 585 (1980); Macromolecules, **14**(2), (1981), in press.
3) R.W. Hendricks and P.W. Schmidt, Acta Phys. Austriaca, **26**, 97 (1967).
4) R.W. Hendricks and P.W. Schmidt, Acta Phys. Austriaca, **37**, 20 (1973).
5) O. Kratky, Z. Elektrochem., **58**, 49 (1954); **62**, 66 (1958); Kolloid-Z., **144**, 110 (1955); O. Kratky and Z. Skala, Z. Elektrochem., **62**, 73 (1958).
6) W.W. Beeman, in "Small-Angle X-ray Scattering", H. Brumberger, Ed., Gordon and Breach, N.Y., 1967, pp. 197.
7) M. Shibayama, M. Fujimura, K. Saijo, S. Suehiro, T. Hashimoto, and H. Kawai, Polym. Prepr., Jpn., **27**, 1652 (1978). T. Hashimoto, S. Suehiro, M. Shibayama, K. Saijo, and H. Kawai, Polym. J., **13** (5), 501 (1981).
8) A. Todo, T. Hashimoto, and H. Kawai, J. Appl. Cryst., **11**, 558 (1978).
9) T. Hashimoto, A. Todo, H. Itoi, and H. Kawai, Macromolecules, **10**, 377 (1977).
10) A. Todo, H. Uno, K. Miyoshi, T. Hashimoto, and H. Kawai, Polym. Eng. & Sci., **17**, 587 (1977).
11) T. Hashimoto, M. Shibayama, and H. Kawai, Macromolecules, **13**, 1237 (1980).
12) T. Hashimoto, M. Fujimura, and H. Kawai, Macromolecules, **13**, 1660 (1980).